RSC Advances

PAPER

View Article Online
View Journal | View Issue

Cite this: *RSC Adv.*, 2017, **7**, 55489

Preparation of multifunctional Fe_3O_4@$ZnAl_2O_4$:Eu^{3+}@mSiO_2–APTES drug-carrier for microwave controlled release of anticancer drugs†

Yumei Bu,[a] Bin Cui,*[a] Weiwei Zhao[ab] and Zhenfeng Yang[a]

Received 1st November 2017
Accepted 24th November 2017

DOI: 10.1039/c7ra12004d

rsc.li/rsc-advances

A carrier possessing simple structure and composition, but with microwave-targeted-fluorescence multifunctional properties to precisely control the delivery of the drug was prepared. Herein, we have constructed the multifunctional Fe_3O_4@$ZnAl_2O_4$:Eu^{3+}@mSiO_2–APTES core–shell drug-carrier *via* direct precipitation method and sol–gel process with surfactant-assistance approach. This carrier is a monodisperse microsphere with an average particle size of 325 nm. Fe_3O_4 in the core has a high saturation magnetization and provides the Fe_3O_4@$ZnAl_2O_4$:Eu^{3+}@mSiO_2–APTES with good drug targeting properties. The $ZnAl_2O_4$:Eu^{3+} interlayer has the characteristic of fluorescent luminescence and can be used to monitor the transport of drugs in the body in real time. In addition, the $ZnAl_2O_4$:Eu^{3+} as a dielectric loss microwave absorbing material combines with the high magnetic loss Fe_3O_4 to form a composite material, which improved the microwave thermal response. Over 78.2% of VP16 molecules were released under microwave trigger. In addition, mesoporous silica nanoparticles in the outer layer improve the drug loading efficiency through organic modification. The results indicated that this multifunctional drug-carrier with simple structure and composition is a potential controlled drug delivery system in cancer therapy.

Introduction

Targeted drug delivery systems with magnetic targeting and fluorescence monitoring have been extensively studied in cancer treatment.[1–3] In order to achieve the purpose of targeted therapy, the drug-targeted delivery systems would not only increase the drug loading efficiency but also reduce the side effects of drugs on normal cells. Recently, mesoporous silica nanoparticles have become one of the best prospective carriers. For example, Yao *et al.*[4] prepared a multifunctional composite of mesoporous silica nanoparticles capped with graphene quantum dots, which has potential for synergistic chemo-photothermal therapy. Researchers[5,6] also found that they can improve the drug loading efficiency through organic modification of nanoparticles with amino, carboxyl groups, hydroxyl groups, *etc*, so as to obtain drug molecules attached to nanometer-size carriers in a particular reaction such as hydrogen bonding, van der Waals force, *etc.*

The amount of released drug is also a key problem in treating cancer effectively. The methods of controlling drug release include response *in vitro* release and *in vivo* release. Response release in the body primarily depends on a high concentration of some enzymes, the redox environment and the influence of pH value.[7,8] The response release *in vitro* refers to the carriers responding to external stimuli, such as ultrasound, alternating electric field, alternating magnetic field, infrared irradiation, and microwave triggers.[9,10] Comparing both the controlled drug release methods, targeting carrier research with *in vitro* stimulation has attracted more attention. Temperature response of controlled drug release has received much interest, and great progress in controlled drug release has been made in this area.[11] The traditional temperature-controlled drug release includes infrared light heating and alternating magnetic field heating. Recently, microwave radiation heating has achieved good research results. Our research group conducted some research work on microwave radiation controlled drug release; the involved microwave materials included ZnO, TiO_2, SnO_2 and WO_3.[5,12–14] Although the prepared nanocarriers possessed multifunctional properties, their composition and structure are relatively complex. For example, Qiu *et al.*[20] constructed the core–shell structured Fe_3O_4@ZnO@mGd_2O_3:Eu@P(NIPAM-*co*-

[a]*Key Laboratory of Synthetic and Natural Functional Molecule Chemistry (Ministry of Education), Shaanxi Key Laboratory of Physico-Inorganic Chemistry, College of Chemistry & Materials Science, Northwest University, 1 Xuefu Ave., Chang'an District, Xi'an, Shaanxi 710127, P. R. China. E-mail: cuibin@nwu.edu.cn; Tel: +86 29 8153 5030*

[b]*Department of Chemistry and Chemical Engineering, Baoji University of Arts and Sciences, Baoji, Shaanxi 721013, P. R. China*

† Electronic supplementary information (ESI) available. See DOI: 10.1039/c7ra12004d

MAA) multifunctional nanocarrier, which combines the properties of magnetic response, microwave thermal response, fluorescence and mesoporosity, but requires three layers of different materials. Each material can only play a single role; thus, the construction of the carrier needs more types of materials, and is costly and time-consuming.

The composite oxide zinc aluminate ($ZnAl_2O_4$) is a very good microwave heat response material. Compared to the simple oxides mentioned above, $ZnAl_2O_4$ has high chemical stability and resistance.[15] In particular, it can enhance the microwave thermal response performance when combined with Fe_3O_4, and would also have good fluorescence after doping with Eu^{3+}.[16] Therefore, $ZnAl_2O_4$:Eu^{3+} has both microwave thermal response and fluorescence properties and can simplify the composition and preparation process of a drug-carrier. Herein, we prepared a new type of carrier Fe_3O_4@$ZnAl_2O_4$:Eu^{3+}@$mSiO_2$–APTES (denoted as FZAM–APTES) for the first time. The synthesis route of FZAM–APTES particles, drug loading and controlled release under a microwave trigger are presented in Scheme 1. Fe_3O_4 in the core endows excellent targeting to the carrier and also can enhance the microwave thermal response performance when combined with the $ZnAl_2O_4$. The layer of $ZnAl_2O_4$:Eu^{3+} not only endows it with microwave thermal conversion properties but also achieves the fluorescence monitoring in real time. In addition, the mesoporous silica nanoparticles and APTES in the outer layer are used for improving the drug loading efficiency. Drugs possessing hydroxyl and carboxyl functional groups would form intermolecular hydrogen bonds with NH_2 of APTES; subsequently, they could be loaded into a drug carrier. Such drugs include etoposide (VP16), ibuprofen, and MPT.[13,17] Among them, VP16 is the most commonly used anticancer model drug. Hence, we chose the anticancer drug VP16 as the model drug to investigate the drug loading and releasing processes and investigated the controlled drug release through microwave radiation response. This multifunctional composite with a simple structure and composition would possess potential application in targeted drug delivery, fluorescence monitoring and microwave controlled release in biomedicine.

Material and methods

Reagents

Sodium citrate ($Na_3C_6H_5O_7 \cdot 2H_2O$, purity ≥ 98.0%), ferric chloride hexahydrate ($FeCl_3 \cdot 6H_2O$), 3-aminopropyltriethoxysilane ($C_9H_{23}NO_3Si$, APTES, purity > 99.0%) and sodium acetate (CH_3COONa, purity > 99.0%) were purchased from the Shanghai Chemical Reagent Factory. Cetyltrimethylammonium bromide (CTAB) was purchased from Sigma-Aldrich. Anhydrous ethanol was purchased from Xi'an Chemical Regent Company. Tetraethyl orthosilicate (TEOS) was purchased from Tianjin Chemical Co., Ltd. of China. Etoposide (VP16, purity > 99.0%) was purchased from Shanghai Adamas Reagent Co., Ltd. Zinc nitrate hexahydrate ($Zn(NO_3)_2 \cdot 6H_2O$, purity > 99.0%), aluminum nitrate ($Al(NO_3)_3 \cdot 9H_2O$, purity > 99.0%), and europium(III) nitrate hexahydrate ($Eu(NO_3)_3 \cdot 6H_2O$, purity > 99.0%) were obtained from Aladdin Industrial Corporation (Shanghai, China). Other chemicals were purchased from National Pharmaceutical Group Chemical Reagent Co., Ltd.

Synthesis of Fe_3O_4@$ZnAl_2O_4$:Eu^{3+}, Fe_3O_4@$ZnAl_2O_4$:Eu^{3+}@$mSiO_2$–APTES drug-carrier

Fe_3O_4@$ZnAl_2O_4$:Eu^{3+} (denoted as FZA) was prepared according to the following experimental procedure. Fe_3O_4 nanoparticles with a diameter of about 260 nm were synthesized as previously reported.[18] Fe_3O_4 nanoparticles (0.1 g) were added to distilled water (20 mL), followed by ultrasonic treatment for 10 min. Then, the pH of the solution was adjusted to 10 with ammonia. Then, the following mixed solution of $Zn(NO_3)_2 \cdot 6H_2O$ (2 mmol), $Al(NO_3)_3 \cdot 9H_2O$ (4 mmol) and $Eu(NO_3)_3$ (0.04 mmol) was dissolved in 20 mL ethylene glycol and added to the previous

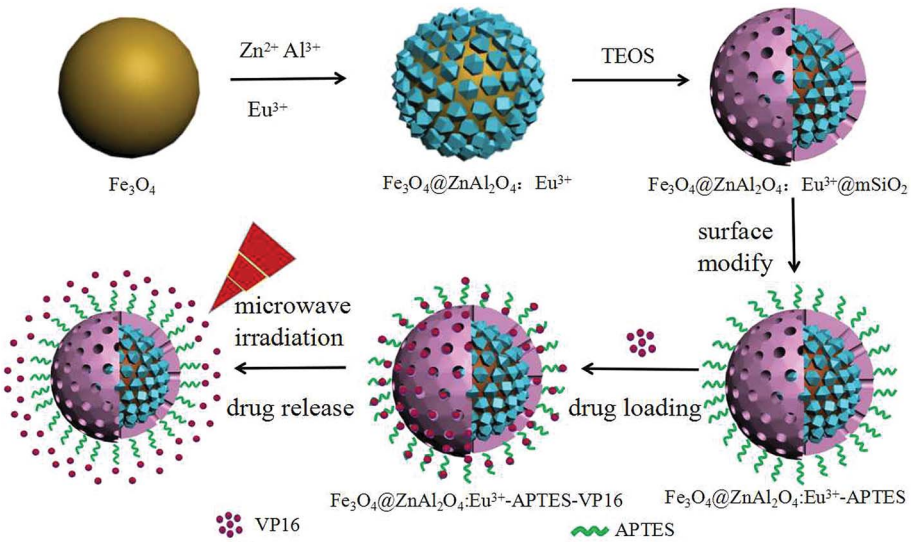

Scheme 1 Schematic illustration of the preparation process of the Fe_3O_4@$ZnAl_2O_4$:Eu^{3+}@$mSiO_2$–APTES and drug loading and release controlled under microwave irradiation.

solution under magnetic stirring for 4 h at 60 °C. Next, the above solution was transferred to an autoclave equipped with a polytetrafluoroethylene liner, placed in an oven, and heated to 200 °C for 24 h. After the reaction was completed, the autoclave was cooled to room temperature. Then, the precipitate was collected and washed several times with deionized water and ethanol. Finally, the precipitate was dried in an oven at 80 °C for 4 h to obtain Fe_3O_4@$ZnAl_2O_4$:Eu^{3+} composite.[19]

Furthermore, FZAM–APTES nanoparticles were synthesized according to the previously reported procedure by coating a mesoporous silica layer and modifying APTES on the surface of FZA.[18]

Model drug loading experiment

We chose VP16 as the model drug and carried out the drug loading and releasing experiments *in vitro*. For VP16 loading, the method has been described in a previous paper.[21] VP16 (25 mg) was dissolved in 50 mL physiological saline (0.9% w/v, similar to the normal physiological environment of the human blood system) to obtain a drug concentration of 0.5 mg mL^{-1}. Then, this solution was mixed with 0.2 g FZAM–APTES to form a suspension. Following this, the suspension was gently stirred at 37 °C and 1 mL of supernatant was removed at appropriate intervals. After 24 h, the collected supernatant was subjected to UV testing to calculate the amount of drug loaded into FZAM–APTES and the percentage of loading.

Microwave thermal response test and model drug release experiment

The microwave thermal response test was carried out according to the previous study.[22] Initially, 0.2 g of FZAM–APTES was dispersed in 40 mL of physiological saline at room temperature. Then, the suspension was irradiated by microwave at a frequency of 2.45 GHz (which is in range for biomedical applications). The temperature of the suspension was measured every 20 s and the total microwave trigger time was 100 s. In addition, 40 mL of Fe_3O_4 and FZA suspension and 40 mL of physiological saline were used as controls.

In order to investigate the controlled drug release property of FZAM–APTES under the microwave trigger, we conducted the control trials: one with microwave trigger, and the other with stirring at 37 °C without microwave trigger. FZAM–APTES–VP16 composites were dispersed in 50 mL physiological saline, then treated with microwave trigger and stirring. For each cycle, the suspension was irradiated with microwave for 15 min, 1 mL supernatant was removed, and 1 mL of physiological saline was added to maintain the volume of solution at 50 mL. Then, the solution was stirred at 37 °C for 15 min, followed by removal of 1 mL supernatant. After seven cycles, the concentration of the drug in the supernatant was measured by a UV-vis spectrophotometer to calculate the released amount of drug.

Characterization

The phase composition of the samples was characterized by a D8 Advance X-ray diffractometer (XRD; Bruker, Germany) using Cu Kα radiation (Kα = 1.54059 Å) at room temperature. The UV-vis adsorption spectral values were measured on a UV-3100 spectrophotometer (Hitachi, Japan) by detecting the amount of drug in the supernatant that was not loaded into the carrier. The morphologies and structures of the as-prepared samples were inspected using a transmission electron microscope (TEM; FEI, Tecnai G2 F20 S-TWIN). Fourier-transform infrared (FT-IR) spectra were obtained using a Tensor-27 infrared spectrophotometer (Bruker) with the KBr pellet technique. The emission spectra of the samples were recorded with a Hitachi (Tokyo, Japan) F-4500 fluorescence spectrometer. Nitrogen adsorption/desorption analysis was measured at liquid nitrogen temperature (77 K) using a Micromeritics ASAP 2010M instrument. The measurements of magnetic properties, microwave thermal response properties and control of drug release with microwave irradiation were performed on a vibrating-sample magnetometer (VSM, Quantum Design, MPMS-XL-7) and the WF-4000 microwave reaction system (Preekem, China) with working frequency of 2.45 GHz. The above measurements were performed at room temperature.

Results and discussion

Phase, morphology and structure of as-prepared FZAM-APTES drug-carrier

Fig. 1 shows the XRD patterns of samples FZA and FZAM–APTES. It can be deduced that there are cubic spinel Fe_3O_4 (JCPDS, card no. 19-0629) and cubic $ZnAl_2O_4$ (JCPDS, 05-0669) present in FZA and FZAM–APTES, respectively. After coating of SiO_2 (Fig. 1b), the slightly raised broad peak in the XRD pattern around 23° can be assigned to the amorphous SiO_2 shell of FZAM–APTES (marked as ●).[23] Compared to FZA, the XRD patterns of FZAM–APTES did not display additional miscellaneous peaks, indicating that there is no other chemical reaction occurring between the core and the shell in the formation process of the drug carrier.

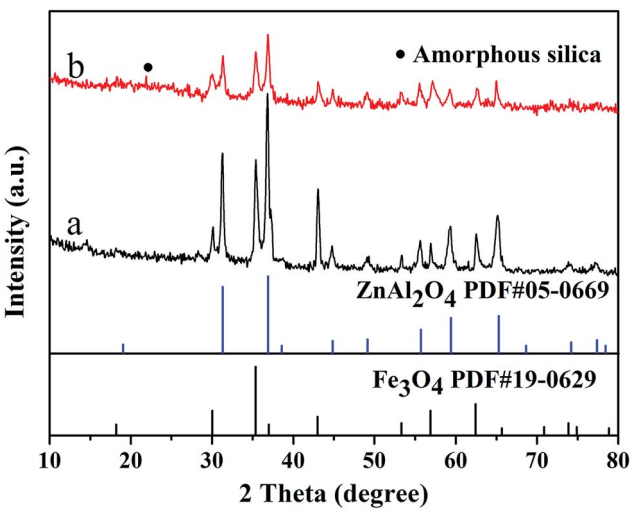

Fig. 1 The XRD patterns of (a) FZA particles and (b) FZAM–APTES microspheres.

Fig. 2 shows the TEM image and EDS of as-prepared Fe_3O_4, FZA and FZAM–APTES microspheres. Fig. 2a is the TEM image of Fe_3O_4. It is clearly demonstrated that the Fe_3O_4 nanoparticles are spherical and display good monodispersity with a diameter of about 260 nm. As shown in Fig. 2b, we can clearly observe a $ZnAl_2O_4$ nanocrystal layer. The grain size is about 25 nm with good dispersion. Fig. 2c represents the HRTEM image of FZA and the inset of Fig. 2b is the dark field image of FZA. In this image, we can also observe a $ZnAl_2O_4$ nanocrystal layer coated on the surface of Fe_3O_4 nanoparticles. Fig. 2d–f represent the TEM images of FZAM–APTES under different magnifications. From the contrast of the pictures we can conclude that we have successfully coated a uniform mesoporous silica layer of about 50 nm on the outer surface of FZA. From the energy-dispersive spectra (Fig. 2g) we can observe the five main elements of Fe, Zn, Al, Si, and Eu in FZAM–APTES composites. Further, in the line scanning images (line 1 and 2) shown in Fig. 2h, the broad peak of Fe element in the core corresponds to Fe_3O_4 nanoparticles. The sharp peaks of the Si element at the edge indicate the SiO_2 layer located on the outermost surface of the nanoparticle. In addition, the two small peaks of Al and Zn elements between the peaks of Fe and Si prove that $ZnAl_2O_4$ is the middle shell of FZAM–APTES composites and the thickness is about 25 nm. This suggests that we have coated a layer of $ZnAl_2O_4$:Eu^{3+} on the surface of Fe_3O_4 nanoparticles and then formed a mesoporous silica layer on the outer surface of the $ZnAl_2O_4$:Eu^{3+} layer. Thus, we have successfully prepared a core–shell structure drug-carrier of Fe_3O_4@$ZnAl_2O_4$:Eu^{3+}@$mSiO_2$–APTES.

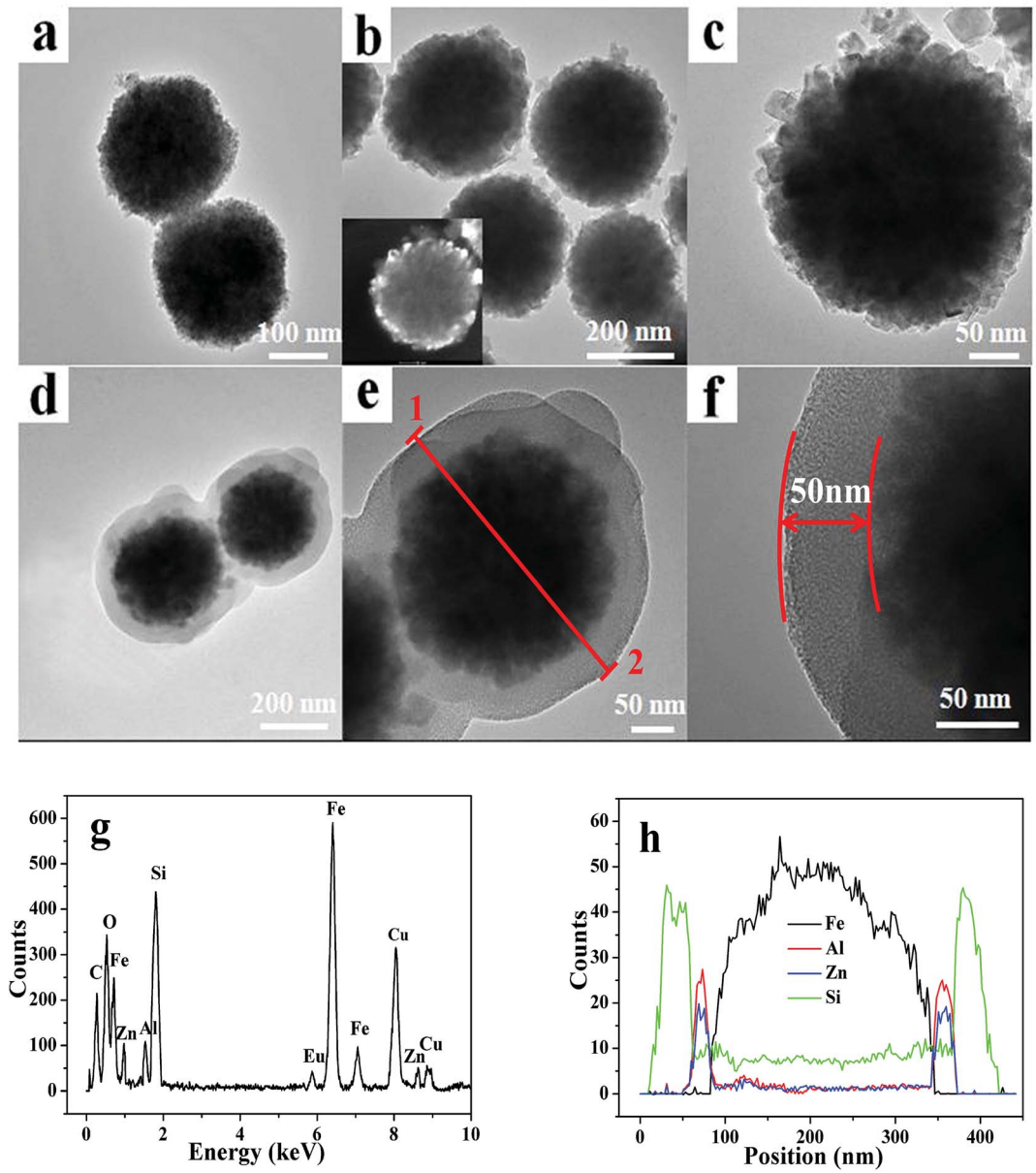

Fig. 2 TEM image of Fe_3O_4 (a), FZA (b), HRTEM image of FZA (c), different magnifications of FZAM–APTES microspheres (d–f), energy-dispersive spectrometry (EDS) (g), and line scanning (line 1 and 2) images (h) of FZAM–APTES.

The mesoporous property of the FZAM–APTES drug-carrier is similar to the Fe_3O_4@SiO_2@mSiO_2 carrier (as shown in Fig. S1 of ESI†),[18] which has a high BET surface area and a total pore volume of 518.60 $cm^2\ g^{-1}$ and 0.275 $cm^3\ g^{-1}$, respectively, and also has an average pore size of 2.43 nm. The obtained results proved that the mesoporous silica layer has been coated on the outer surface of FZA using CTAB as a template to form the pore structure.[24] Therefore, the as-prepared carrier possesses a larger drug loading space that can greatly increase drug-loading.

Magnetic, photoluminescent and microwave thermal response properties of samples

The magnetization saturation (M_s) values for Fe_3O_4, FZA and FZAM–APTES–VP16 are 86.8, 58.4 and 17.4 emu g^{-1}, respectively (as shown in Fig. S2†).[24] It can be observed that compared with the saturation magnetization of Fe_3O_4, those of FZA and FZAM–APTES–VP16 were significantly reduced. This can be due to the introduction of $ZnAl_2O_4$:Eu^{3+} and mSiO_2, decreasing the mass fraction of magnetic Fe_3O_4. In addition, this result also revealed that FZAM–APTES–VP16 exhibits good magnetic response, which would have potential applications in targeting and separation.[6]

In order to study the luminescent properties of the prepared drug carrier, we carried out the excitation spectrum and emission spectrum tests at room temperature; the results are shown in Fig. 3. The typical excitation spectrum (Fig. 3a) consists of a strong band at 252 nm, a sharp band at 398 nm and a wide weak band at 466 nm at $\lambda_{em} = 614$ nm. The strong absorption band at 252 nm is caused by the charge-transfer band (CTB) between the 2p orbital of O^{2-} and the 4f orbital of Eu^{3+} ions, while the excitation peaks at 398 and 466 nm correspond to the energy level transitions of Eu^{3+} for $^7F_0 \rightarrow {}^5D_3$ and $^7F_0 \rightarrow {}^5D_2$, respectively.[25] In addition, the typical emission spectra of FZA, FZAM–APTES and FZAM–APTES–VP16 composites under excitation of 398 nm ultraviolet light are shown in Fig. 3b. A series of sharp bands at 576, 589, 611, 649 and 699 nm can be assigned to the energy level transition of Eu^{3+} from $^5D_0 \rightarrow {}^7F_j$ ($j = 0, 1, 2, 3$ and 4). Among them, the most intense emission peak at 611 nm corresponds to $^5D_0 \rightarrow {}^7F_2$, usually occurring through the forced electric dipole transition. Moreover, the broad band at 452 nm (Fig. 3b) was caused by the lattice host of $ZnAl_2O_4$.[18] The intensities for FZAM–APTES and FZAM–APTES–VP16 were decreased compared with FZA. This could be because the layers of mesoporous silica, APTES and the drug molecule weaken the content of $ZnAl_2O_4$:Eu^{3+}, but it is still strong enough to be useful in real-time monitoring of the drug location.

The time–temperature curves of physiological saline, Fe_3O_4, FZA and FZAM–APTES under microwave trigger are shown in Fig. 4. From the curves, we can observe that the four samples exhibit different microwave thermal responses. The thermal response rate is physiological saline < Fe_3O_4 < FZAM–APTES < FZA. The initial temperature of the test system was 14.5 °C and that for FZAM–APTES rose to 46.6 °C in 100 s. However, the temperatures of the pure physiological saline and Fe_3O_4 mixed solution reached 35.8 and 41.4 °C in 100 s, respectively, which is a relatively poor microwave thermal response. These results indicate that FZA and FZAM–APTES composites possess good microwave thermal conversion performance; they took 100 s to reach 51.5 and 46.6 °C, respectively. $ZnAl_2O_4$:Eu^{3+} as the

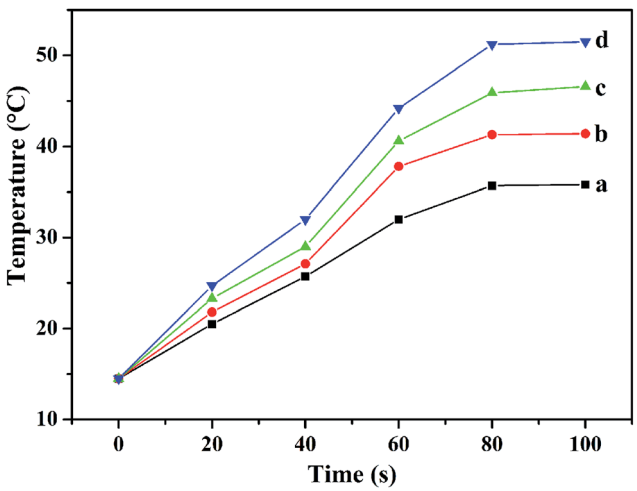

Fig. 4 The microwave thermal response of time-dependent temperature curve for the sodium chloride solution (a), and Fe_3O_4 (b), FZAM–APTES (c) and FZA (d) dispersed in sodium chloride solution with microwave irradiation at 2.45 GHz.

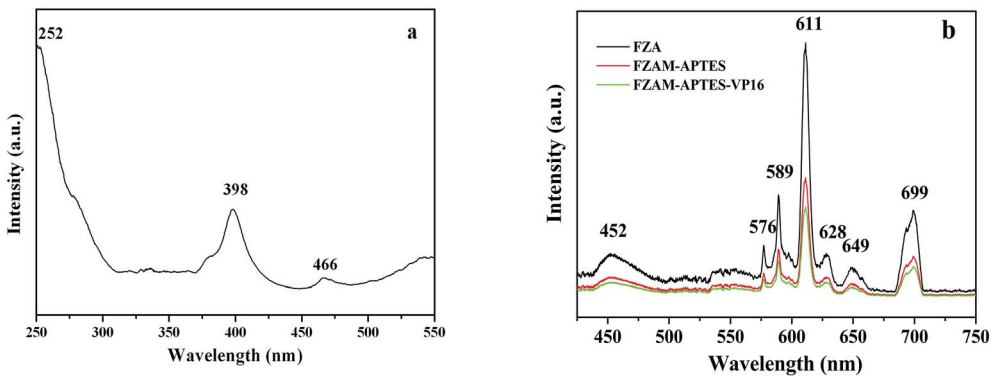

Fig. 3 Excitation spectrum of the FZA nanoparticles at $\lambda_{em} = 614$ nm (a); emission spectra of FZA, FZAM–APTES and FZAM–APTES–VP16 nanoparticles at $\lambda_{ex} = 398$ nm (b).

common component of these two composites, is a good microwave absorption material,[26] and under the same conditions $ZnAl_2O_4$:Eu^{3+} can quickly convert electromagnetic energy into heat. The reduction in microwave thermal conversion compared with FZA could be attributed to the lower mass fraction of $ZnAl_2O_4$:Eu^{3+} component in the FZAM–APTES composite because the mesoporous silica and APTES in the carrier would dilute the concentration of $ZnAl_2O_4$:Eu^{3+} composite. However, FZAM–APTES still exhibits significant microwave absorption effect. Therefore FZAM–APTES, as a drug carrier, has an excellent microwave thermal response property and can absorb microwaves and convert them to thermal energy.

Drug loading and release properties

The structure of FZAM–APTES is similar to the Fe_3O_4@WO_3@-$mSiO_2$ composite, which was prepared earlier by our group.[14] Both composites are coated with $mSiO_2$ on the outer layer and then modified with APTES. Therefore, their drug loading mechanisms and processes are similar. Approximately 91.8% of the total VP16 drug solution was adsorbed and loaded into the mesoporous layer of FZAM–APTES composite particles (as shown in Fig. S4†). In the FT-IR spectra of the composite (Fig. S3b and c†), the absorption bands at 566 and 680 cm^{-1} were assigned to $ZnAl_2O_4$ particles of the regular spinel structure,[27] which proved that $ZnAl_2O_4$:Eu^{3+} composite was successfully coated on the surface of Fe_3O_4. In the infrared spectrum of VP16 (Fig. S3a†) and FZAM–APTES–VP16 (Fig. S3b†), the absorption peak at 1481 cm^{-1} was the characteristic vibration peak of C=C of the aromatic skeleton of VP16. The IR absorption peak at 1763 cm^{-1} was the characteristic peak of the stretching vibration of C=O. This further confirms that VP16 was successfully linked to the pores of the mesoporous SiO_2 shell of FZAM–APTES nanoparticles. Specific information is displayed in the ESI.†

From the above microwave heat transfer test results of the samples, we can observe that the FZAM–APTES drug-carrier has an excellent microwave thermal response property. The release behavior of VP16 molecules from the carrier FZAM–APTES under microwave irradiation and stirring at 37 °C without microwave irradiation are shown in Fig. 5. We can observe that after the first stage of microwave irradiation for 15 min, about 20% of the drug was released from the FZAM–APTES–VP16 solution, but only 1% of the drug was released with stirring without microwave trigger, which shows that our as-prepared composite could enable the quick release of drug under microwave irradiation. However, after the microwave was turned off, the release of the VP16 molecules was inhibited. These results indicate that the release of drug molecules can be precisely controlled by adjusting the microwave on/off states and irradiation time. With the increase of time, the release curve tends to be gentle, and approximately 78.2% of the drug was released from the drug carrier after seven cycles. We can conclude that FZAM–APTES has improved sustained performance and can significantly control the release of VP16. This could be due to microwave thermal response related to the irradiation time; as the time increased, the effect of microwave thermal response enhanced and the temperature of the sample also increased. Combined with the conclusion from the microwave thermal response (Fig. 4), we know that high temperature is favorable for fast molecular diffusion through the pore channels. Thus, the cumulative release rate of VP16 molecules increased with the increase in duration of the microwave trigger. This indicates that FZAM–APTES can be used as a highly efficient drug carrier to control drug release with a microwave trigger.

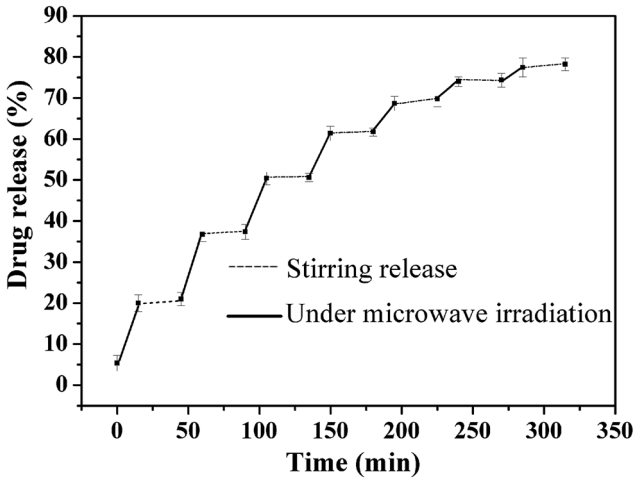

Fig. 5 Controlled release of VP16 from FZAM–APTES–VP16 under microwave irradiation and stirring for seven release cycles.

Conclusions

We successfully synthesized the novel multifunctional Fe_3O_4@$ZnAl_2O_4$:Eu^{3+}@$mSiO_2$–APTES core–shell structured composite by combining the direct precipitation method and sol–gel process with the surfactant-assistance approach. The $ZnAl_2O_4$:Eu^{3+} located in the middle layer of the drug-carrier, as a microwave thermal responsive material, contributes to microwave triggered drug release. It was also discovered that the composite particles emit a strong fluorescence emission peak by monitoring the excitation wavelength at 398 nm. This proved that the drug carrier possesses fluorescence emission properties and can lay the experimental foundation for clinical fluorescence monitoring *in vivo*. In addition, the drug release of this carrier can be effectively controlled by microwave stimulation as over 78.2% of the total VP16 was released under discontinuous microwave irradiation for seven cycles. Therefore, we have obtained a multifunctional drug-carrier possessing simple structure and composition with simultaneous targeted microwave thermal response and fluorescence monitoring performance.

Conflicts of interest

There are no conflicts to declare.

Acknowledgements

This project is financially supported by the National Natural Science Foundation of China (grant No. 21071115), the Education Committee of Shaanxi Province (grant number 16JS112), Shaanxi Natural Science Foundation Project (grant number 2016JZ006) and Shaanxi Light Optoelectronics Material Co., Ltd.

Notes and references

1 J. Long, G. Luo, Z. Xiao, Z. Liu, M. Guo, L. Liu, C. Liu, J. Xu, Y. Gao, Y. Zheng, C. Wu, Q. Ni, M. Li and X. Yu, *Cancer Lett.*, 2014, **346**, 273–277.
2 P. Ai, H. Wang, K. Liu, T. Wang, W. Gu, L. Ye and C. Yan, *RSC Adv.*, 2017, **7**, 19954–19959.
3 P. Xi, K. Cheng, X. Sun, Z. Zeng and S. Sun, *Chem. Commun.*, 2012, **48**, 2952–2954.
4 X. Yao, Z. Tian, J. Liu, Y. Zhu and N. Hanagata, *Langmuir*, 2017, **33**, 591–599.
5 Y. Chen, H. Zhang, X. Cai, J. Ji, S. He and G. Zhai, *RSC Adv.*, 2016, **6**, 92073–92091.
6 K. Can, M. Ozmen and M. Ersoz, *Colloids Surf., B*, 2009, **71**, 154–159.
7 J. W. Cui, Y. J. Yan, Y. Wang and F. Caruso, *Adv. Funct. Mater.*, 2012, **22**, 4844.
8 X. Yao, X. Zheng, J. Zhang and K. Cai, *RSC Adv.*, 2016, **6**, 76473–76481.
9 G. Feng, L. Han, C. Y. Xu, Y. Zheng, P. Li, Y. Cao, Q. Wang, J. Xia and Z. Wang, *Int. J. Nanomed.*, 2017, **12**, 4647–4659.
10 Y. Lin, Y. Yu, S. Wang and R. Lee, *RSC Adv.*, 2017, **7**, 43212–43226.
11 A. Riedinger, P. Guardia, A. Curcio, A. Riedinger, P. Guardia, A. Curcio, M. A. Garcia, R. Cingolani, L. Manna and T. Pellegrino, *Nano Lett.*, 2013, **13**, 2399–2406.
12 H. Peng, C. Hu, J. Hu, T. Wu and X. Tian, *J. Sol–Gel Sci. Technol.*, 2016, **80**, 133–141.
13 H. Peng, B. Cui, W. Zhao, X. Zhao, Y. Wang, Z. Chang and Y. Wang, *New J. Chem.*, 2016, **40**, 1460–1470.
14 W. Zhao, B. Cui, H. Qiu, P. Chen and Y. Wang, *Mater. Lett.*, 2016, **169**, 185–188.
15 P. Fu, Z. Wang, Z. Lin, Y. Liu and A. R. Vellalsamy, *J. Mater. Sci.: Mater. Electron.*, 2017, **13**, 9589–9595.
16 I. Kaminska, K. Fronc, B. Sikora, K. Koper, R. Minikayev, W. Paszkowicz, K. Sobczak, T. Wojciechowski, M. Chwastyk, A. Reszka, B. J. Kowalski, P. Stepien and D. Elbaum, *RSC Adv.*, 2014, **4**, 56596–56604.
17 R. Mitran, C. Matei and D. Berger, *J. Phys. Chem. C*, 2016, **120**, 29202–29209.
18 W. Zhao, B. Cui, H. Peng, H. Qiu and Y. Wang, *J. Phys. Chem. C*, 2015, **119**, 4379–4386.
19 X. Chen, C. Ma, S. Bao and Z. Li, *J. Colloid Interface Sci.*, 2010, **346**, 8–11.
20 H. Qiu, B. Cui, W. Zhao, P. Chen, H. Peng and Y. Wang, *J. Mater. Chem. B*, 2015, **3**, 6919–6927.
21 D. Long, T. Liu, L. Tan, H. Shi, P. Liang, S. Tang, Q. Wu, J. Yu, J. Dou and X. Meng, *ACS Nano*, 2016, **10**, 9516–9528.
22 D. Qu, Y. Ma, W. Sun, Y. Chen, J. Zhou, C. Liu and M. Huang, *Int. J. Nanomed.*, 2015, **10**, 1173–1187.
23 P. Yang, Z. Quan, Z. Hou, C. Li, X. J. Kang, Z. Cheng and J. Lin, *Biomaterials*, 2009, **30**, 4786–4795.
24 H. Qiu, B. Cui, G. Li, J. Yang, H. Peng, Y. Wang, N. Li, R. Gao, Z. Chang and Y. Wang, *J. Phys. Chem. C*, 2014, **118**, 14929–14937.
25 X. Y. Chen and C. Ma, *Opt. Mater.*, 2010, **32**, 415–421.
26 X. Ouyang, S. Wu, Z. Wang and Y. Liu, *J. Alloys Compd.*, 2015, **644**, 242–248.
27 L. Kong, X. Yin, F. Ye, Q. Li, L. Zhang and L. Cheng, *J. Phys. Chem. C*, 2013, **117**, 2135–2146.